ACS Biomaterials SCIENCE & ENGINEERING
Article
Cite This: ACS Biomater. Sci. Eng. 2019, 5, 4985−4993
pubs.acs.org/journal/abseba

# Recombinant Pyriform Silk Fiber Mechanics Are Modulated by Wet-Spinning Conditions

Jeffrey R. Simmons,[†] Lingling Xu,[†] and Jan K. Rainey*[,†,‡]

[†]Department of Biochemistry & Molecular Biology and [‡]Department of Chemistry, Dalhousie University, Halifax, Nova Scotia B3H 4R2, Canada

Supporting Information

**ABSTRACT:** Pyriform silk is a critically important fiber in spider web construction. It functions in a glue-coated attachment disc to form junctions in spider webs, connecting the web to disparate materials. Despite the biological importance of this silk, both natural and recombinant pyriform silk have yet to be structurally or mechanically characterized. In this study, we demonstrate recombinant production of a 477 amino acid protein based on *Argiope argentata* pyriform silk. This pyriform silk protein shows α-helicity in both an aqueous buffer and in a fluorinated acid- and alcohol-based spinning dope. Wet-spinning produced fibers having no visible defects in surface or cross-sectional analysis, with mechanical behavior varying as a function of postspin stretching conditions and correlating to loss of α-helicity in the fibrous state. Multiple conditions gave rise to fibers that are both strong and extensible, contrasting with some other silks that are biased toward being strong or extensible. This behavior is strikingly similar to recombinant aciniform silk, despite distinct primary structuring and composition.

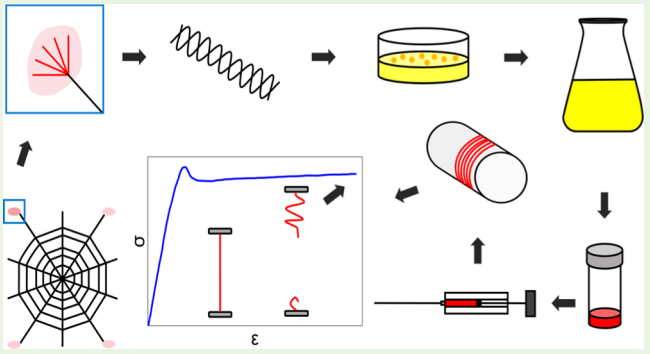


**KEYWORDS:** *recombinant pyriform silk, silk protein structure and morphology, wet-spinning and automated postspin draw, strong and extensible fibers, tunable mechanical properties*



## INTRODUCTION

There are seven well-established classes of silk employed by spiders for web construction and other functions.[1] Each type of silk serves a unique purpose, from providing extensibility, protecting against wind, to providing strength, supporting the spider and prey.[2,3] The fiber-forming spider silks, in particular, have received much attention as lightweight biomaterials, with mechanical properties comparable to steel and Kevlar.[4,5]

To date, most studies have focused on a small subset of spider silks. In particular, dragline silk has been the most extensively characterized class of silk. Conversely, pyriform (or piriform) silk has been very sparsely explored. This silk serves as the junction former in spider webs and is the fibrous component of a two-part system called an attachment disc. The other part of the attachment disc is a glue-like material that is produced deeper in the gland and coated onto the pyriform silk fiber during spinning.[6] Strong dipole−dipole and ionic interactions have been proposed as the primary attractive forces holding the glue to silks or other substrates.[7] Architectural differences between attachment discs have been noted both to provide distinct functionality (i.e., substrate attachment vs prey capture[8]) and between species.[9]

Spider silks are primarily formed by proteins termed as spidroins. Pyriform spidroin 1 (PySp1) consists of a tripartite architecture comprising short nonrepetitive N- and C-terminal regions[10] and a core repetitive domain, as seen with other better-characterized spidroins.[11,12] The PySp1 repetitive domain in *Argiope argentata* represents ∼85% of the total protein length,[10] flanked by the nonrepetitive N- and C-terminal domains that are characteristic of spidroins[12,13] by distinctive heterogeneous linkers. Also, unlike the relatively well-studied spidroins comprising major and minor ampullate silks which have repetitive domains composed of relatively short motifs (3−12 amino acids) repeated numerous times in various combinations,[12,14] pyriform spidroin repetitive domains have lengthy repeat units composed of distinct segments that are Gln-rich and Pro-rich. The repeat unit in *A. argentata* PySp1 is 234 amino acids long,[10] which is most comparable in size to the ∼180-amino acid tubuliform[15] and ∼200-amino acid aciniform[11] repeats. The *A. argentata* PySp1 repetitive domain contains distinctive QSXXXQ motifs (X = A, V, or S) in the Gln-rich region, and numerous copies of XP motifs (X = A, R, or V) in the Pro-rich region. Corresponding to its Gln-rich region, pyriform spidroin has a high proportion of Gln relative to other silks.[10] It has also long been recognized to have lower proportions of Gly and Ala than is typical of spidroins other than aciniform silk and the nonfibrous aggregate silk.[1]

**Received:** April 11, 2019
**Accepted:** September 13, 2019
**Published:** September 13, 2019




DOI: 10.1021/acsbiomaterials.9b00504
ACS Biomater. Sci. Eng. 2019, 5, 4985−4993

```
  1 MGHHHHHHSS AQENSFTQSS VAQQSAVAQQ SSVSQQSSAA QQSSVAQSQQ  50
 51 TSYSAATNAG SSVSQSQAIV SSAPVYFNSQ TLTNNLASSL QSLNALNYVS 100
101 NGQLSSSDVA STVARAVAQS LGLSQGSVQN IMSQQLSSIG SGASTSSLSQ 150
151 AIANAVSSAV QGSQAAAPGQ EQSIAQRVNS AISSAFAQLI SQRTAPAPAP 200
201 RPRPAPLPAP APRPRPAPAP RPAPVYAPAP VASQFQASAS SQSSAQENSF 250
251 TQSSVAQQSA VAQQSSVSQQ SSAAQQSSVA QSQQTSYSAA TNAGSSVSQS 300
301 QAIVSSAPVY FNSQTLTNNL ASSLQSLNAL NYVSNGQLSS SDVASTVARA 350
351 VAQSLGLSQG SVQNIMSQQL SSIGSGASTS SLSQAIANAV SSAVQGSQAA 400
401 APGQEQSIAQ RVNSAISSAF AQLISQRTAP APAPRPRPAP LPAPAPRPRP 450
451 APAPRPAPVY APAPVASQFQ ASASSQS                          477
```

**Figure 1.** Amino acid sequence of $HPy_2$. The $His_6$-tag is grey; repeat 1, red; repeat 2, blue; boldface delineates QSXXXQ motifs; and, underline delineates XP motifs.

Despite these primary structural differences, Raman spectromicroscopy implied similar structural characteristics for spidroins in the highly concentrated soluble state (the "dope") within the pyriform, cylindriform, and aciniform silk glands of *Nephila clavipes*.[16] Similar mixed $\alpha$-helical and $\beta$-sheet compositions were also inferred for pyriform and aciniform silk fibers, leading to the proposal that these silks are likely to behave similarly.[16] Currently, the mechanical behavior of pyriform silk remains uncharacterized due to inherent challenges in collecting and isolating natural pyriform silk. Therefore, the fundamental properties of pyriform silk and its degree of similarity, or lack thereof, to other classes of silk remain elusive.

To date, one form of recombinant pyriform silk has been produced based upon the repetitive unit of *N. clavipes* pyriform spidroin (PySp).[17] Consistent with *A. argentata*, segregated Gln-rich (~190 residues) and Pro-rich (~40 residues) regions were identified, with the 190-residue Gln-rich PySp domain being sufficient to allow for wet-spinning. A qualitative increase in fiber extensibility was noted for wet-spun fibers produced using 230-residue protein comprising the Gln-rich domain followed by the Pro-domain. Although shown to be capable of fiber formation, this recombinant silk has not been characterized from a mechanical or structural perspective.

As noted above, the nonrepetitive N- and C- terminal regions associated with the canonical tripartite spider silk architecture are present in natural PySp1.[10] Although the role of pyriform nonrepetitive domains is yet to be determined, they likely function similarly to those in other silk types.[18−21] For simplicity of recombinant protein production and to allow elaboration of features inherent to pyriform spidroin, our current focus is on the core repetitive region. This follows from previous demonstration of wet-spun, silk-like fibers formed using repetitive domain-based constructs for both pyriform[17] and aciniform[22,23] silks.

Here, we employ a recombinant pyriform silk fragment based upon the recent report of the first complete pyriform spidroin gene sequence, PySp1 from *A. argentata*.[10] Using *Escherichia coli*, a ~47.9 kDa recombinant protein comprising a pair of Gln-rich + Pro-rich domain-containing PySp1 repetitive units is efficiently produced. This protein is shown to be amenable to fiber formation through wet-spinning, with differences in fiber stretching conditions leading to variation in mechanical properties. We show that recombinant pyriform silk is comparably strong to recombinant dragline silk produced with a spidroin of similar molecular weight, with greater extensibility than most recombinant spidroins of similar molecular weight or regenerated wet-spun fibroin.

## MATERIALS AND METHODS

**Protein Design and Cloning.** A recombinant protein consisting of two 234-amino acid repeat units (the $Py_2$ construct) was designed based on the repetitive region of the *A. argentata* PySp1.[10] The N- and C-termini of one repeat ($Py_1$) were chosen following three criteria. First, these were selected in regions where the PSIPRED structural algorithm[24,25] did not predict formation of an $\alpha$-helix or a $\beta$-sheet. This was intended to minimize the possibility of deleterious structural perturbation due to the truncation of a secondary structure unit at either the N- or C-terminus of a given recombinant protein construct. Second, sites were chosen to be amenable to seamless ligation of two or more repeat units as previously employed for recombinant aciniform silk.[26] Third, a nucleophilic amino acid at each end of the sequence was included for future intein-splicing applications.[21,27] A DNA sequence encoding for $Py_1$ was synthesized in a pUC57 vector (Bio Basic Canada Inc.; Markham, ON). A double-repeat ($Py_2$; sequence shown in Figure 1) encoding open reading frame was constructed by double digestion and ligation of two $Py_1$ sequences, similarly to previously reported methods.[26] This $Py_2$-encoding sequence was then inserted into a modified pET32 (Novagen; Darmstadt, Germany) vector downstream of a $His_6$ tag (referred to as the $HPy_2$ construct) for protein expression. N- and C-terminal nonrepetitive regions were not included in the present constructs to allow for specific comparison of features to previously reported wet-spun silks lacking N- and C-terminal nonrepetitive regions, including both pyriform[17] and aciniform[22,23] silks. This design feature was chosen in order to allow for more straightforward analysis of the mechanical importance of the sequentially and architecturally distinctive repeat units of the core repetitive domain without the potential for convolution of effects arising from the nonrepetitive termini that tend to be far more similar from silk type to silk type.

**Protein Expression and Purification.** The $HPy_2$ protein was expressed in *E. coli* BL21(DE3) cells, similarly to a previously described protocol.[26] In brief, a starter culture was transferred to fresh Lysogeny broth (LB) medium (1:50, v/v), and allowed to grow at 37 °C until $OD_{600} \approx 0.8$ was achieved. Target protein expression was induced by adding 0.64 mM isopropyl $\beta$-D-1-thiogalactopyranoside (IPTG; Bio Basic Canada Inc.; Markham, ON) and incubated for 16 h at 22.5 °C. Cells were harvested, resuspended with 5 mL/g wet cell weight of native lysis buffer (QIAexpressionist protocol; Siegen, Hilden, Germany), and lysed via a French Pressure Cell Press (American Instrument Company; Silver Spring, MD). The cell lysate was centrifuged (12 000 rcf, 30 min, 4 °C), and the supernatant was discarded. A Triton-X wash was then used to remove insoluble bacterial proteins in the inclusion bodies.[28,29] Specifically, the cell lysate pellet was resuspended with 10 mL/g wet cell weight of inclusion body wash buffer [50 mM potassium phosphate, pH 8, 1% Triton X-100 (Fluka; Sigma-Aldrich, St. Louis, MO) and 2 M urea (Sigma-Aldrich)] homogenized using a tissue grinder, incubated (1 h, room temperature), and centrifuged (12 000 rcf, 30 min, 4 °C). The Triton-X wash was repeated, followed by a 10 mL/g wet cell weight water wash to remove the Triton (10 min, room temperature), and centrifugation (12 000 rcf, 30 min, 4 °C). The pellet was resuspended at 5 mL/g wet cell weight in 100 mM sodium phosphate buffer containing 10 mM Tris·Cl and 8 M urea at pH 8.00 ± 0.05, and centrifuged (12 000 rcf, 30 min, 4 °C), with $HPy_2$ collected in the supernatant. A gradient urea dialysis (4 M, 2 M) was performed by



DOI: 10.1021/acsbiomaterials.9b00504
ACS Biomater. Sci. Eng. 2019, 5, 4985−4993

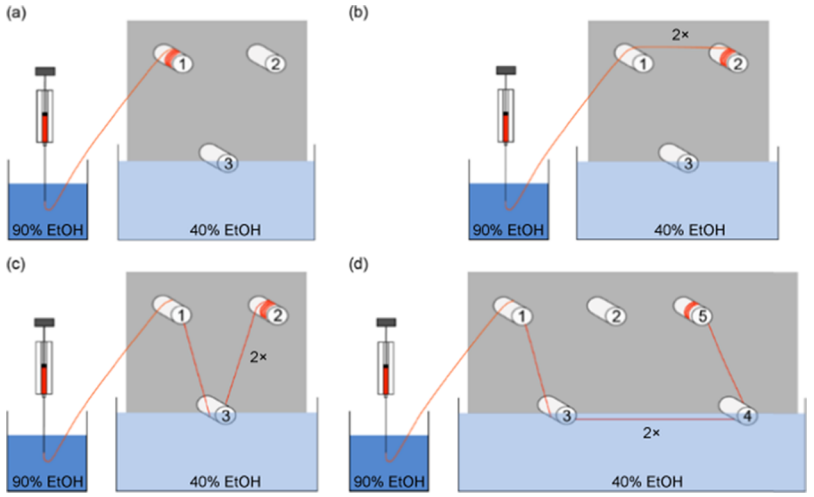


**Figure 2.** Automated wet-spinning postspin stretching apparatus. The spinning dope is placed in a syringe and extruded at a constant rate through a spinneret (illustrated syringe and red dope) into a coagulation bath (dark blue bath). Collection of fibers, using a series of rollers (1−6) with programmable speeds was carried out for AS fiber immediately following coagulation bath (a); following a postspin draw in air (b) vs in a solvent bath (d; light blue bath); and with a postspin draw in air following immersion in solvent (c).

diluting a 50 mM sodium phosphate buffer containing 8 M urea buffer with water, keeping pH adjusted to 8.00 ± 0.05 at each step using solutions of sodium hydroxide (Fisher Chemical; Fair Lawn, NJ) and hydrochloric acid (EMD Chemicals Inc.; Darmstadt, Germany), followed by dialysis against water to remove any remaining salt. The dialyzed solution was then flash frozen with liquid nitrogen, followed by lyophilization (aapptec Sharp Freeze-110, Louisville, KY) to collect the dried protein powder.

**Mass Spectrometry.** $HPy_2$ mass and identity were confirmed by two mass spectrometric methods: intact protein analysis by electrospray ionization+ (ESI+) with ion trap mass spectrometry (MS) analysis and through analysis of protein fragments following in gel digestion. An intact protein sample in 50 mM potassium phosphate buffer was analyzed by liquid chromatography (LC)−MS/MS using a Velos Pro Orbitrap mass spectrometer with an UltiMate 3000 Nano-LC system (Thermo Fisher Scientific; Waltham, MA). In-gel protein digestion was carried out on the major Coomassie-stained SDS-PAGE protein band using sequencing grade chymotrypsin (Roche Diagnostics GmbH; Mannheim, Germany) as detailed previously.[30] Results were analyzed using Proteome Discoverer 2.2 (Thermo Fisher Scientific), searched against the full published PySp1 sequence,[10] *E. coli* proteins, a fasta file corresponding to the $HPy_2$ sequence, and the cRAP (common repository of adventitious proteins) database of common contaminants (Global Proteome Machine Organization).

**Dope Preparation and Viscometry.** The protein powder was dissolved (10% w/v) in trifluoroacetic acid (TFA; EMD Millipore Corporation; Darmstadt, Germany)/2,2,2-trifluoroethanol (TFE; Alfa Aesar; Heysham, UK)/$H_2O$ (3:1:1 v/v/v), a solvent mixture recently shown to solubilize recombinant aciniform silk into a dope for wet-spinning.[23] Following incubation (30 min, room temperature) with intermittent vortexing, the suspension was centrifuged (20 817 rcf, 30 min, 10 °C) and the supernatant retained as the spinning dope. SDS-PAGE was performed on samples obtained before and after each experiment to ensure no significant protein degradation occurred during experiments. Dope viscosity was measured at room temperature using a microVisc HVROC-L portable viscometer using an A05 50 μm flow channel microVisc chip (RheoSense Inc.; San Ramon, CA), as previously detailed.[22] Microviscometer calibration was carried out with deionized water and isopropyl alcohol and the instrument was pre-equilibrated with dope solvent prior to loading the spinning dope. All measurements were carried out at ambient temperature.

**Circular Dichroism Spectroscopy.** A dope sample was prepared at 1% w/v. For comparison, a sample (6.52 μM $HPy_2$) in potassium phosphate buffer was prepared from protein initially resuspended in 8 M urea, 10 mM Tris·Cl, and 100 mM sodium phosphate, dialyzed against a urea gradient (5.1, 3.4, 1.7, 0.8 M, pH 8.00 ± 0.05), followed by dialysis against ∼15 mM potassium phosphate (Fisher Chemical) at pH 7.50 ± 0.05. Far-UV circular dichroism (CD) spectroscopy was performed at 22.5 ± 0.05 °C (Olis DSM20 CD spectrophotometer; Bogart, GA; all optical slits were at a bandpass of 5.0 nm, with ellipticity acquired using integration time as a function of high volts in Olis SpectralWorks version 5.888.272). Spectra were acquired from 250 to 180 nm (1 nm step size) employing quartz cuvettes (0.5 mm path length for buffer samples and 0.01 mm path length for spinning dope samples; Hellma Canada Limited; Concord, ON). The protein concentration in each instance was determined by the Beer−Lambert law using the absorbance at 214 nm.[31] Blank subtraction was performed, and mean residue ellipticity was calculated and averaged ($[\theta]$) for two repetitions. To obtain values for the relative percentage of each type of secondary structure present, CD data in $[\theta]$ format were deconvoluted using the BeStSel algorithm[32,33] (http://bestsel.elte.hu/index.php).

**Fiber Spinning.** Wet-spinning using ∼10% (w/v) $HPy_2$ in TFA/TFE/$H_2O$ (3:1:1 v/v/v) was carried out using an ethanol (EtOH)/water (9:1 v/v) coagulation bath at an extrusion rate of 600 μL/h through a spinneret of 0.127 mm inner diameter, as previously described for aciniform spidroin.[22,23] Fibers were spun at 28.2 ± 2.4% relative humidity and 28.0 ± 2.2 °C, with measurements recorded directly after collection and reported as average ± standard deviation. The recombinant $HPy_2$ fiber formed in the coagulation bath was picked up by tweezers and guided onto a home-built automated spinning apparatus (Figure 2). Fibers were either collected in the as-spun (AS) state on roller 1 (Figure 2a), with collection speed set to match the fiber extrusion speed, or collected following postspin stretching (PS). Postspin stretching was carried out in three distinct ways. For a 2× postspin stretch in air (2× air), as previously employed for *Bombyx mori* silk,[34] the AS fiber was guided onto roller 2 (speed 2× that of roller 1; Figure 2b). For a 2× postspin stretch in air following immersion in EtOH/$H_2O$ (2:3 v/v) (2× after EtOH), the fiber was guided from roller 1 onto roller 3 (speed equal to roller 1) in EtOH/$H_2O$ (2:3 v/v) and collected on roller 2 in air (speed 2× that of roller 1 and 3; Figure 2c). Finally, for a 2× postspin stretch in ethanol (2× in EtOH), the AS fiber was guided from roller 1 onto roller 3 (same speed as roller 1) and then stretched in an EtOH/$H_2O$ (2:3 v/v) bath by passing over roller 4 (speed 2× that of roller 1 and 3) followed by collection on roller 5 (speed equal that of roller 4) in air (Figure 2d).

**Fiber Imaging.** Following spinning, fibers were allowed to dry overnight (room temperature) and secured to U-shaped paper holders



DOI: 10.1021/acsbiomaterials.9b00504
ACS Biomater. Sci. Eng. 2019, 5, 4985−4993

(window size ~1 cm per side) with a 1 cm gap, as previously described.[22,23] Optical microscopy at 100× magnification (Axio Observer A1; Carl Zeiss Canada; Toronto, ON) was performed, with 3 micrographs acquired per fiber (two at either end and one in the middle). Fiber diameters were determined as the average of the diameter at six positions per image using ImageJ 1.51j8, as previously reported,[22] rejecting fibers with visual defects for subsequent analysis. Polarized light microscopy was performed using an Axio Observer A1 equipped with a rotatable stage, a fixed analyzer slider, and a 90° rotatable polarizer D (Carl Zeiss Canada). Fibers were rotated to ~45° relative to the polarized light through direct adjustment and angular measurement prior to image capture. Light intensity and camera angle were standardized to allow for direct comparison between samples.

Scanning electron microscopy (SEM) samples were prepared in a similar manner as done previously.[22] Namely, fibers for surface imaging were transferred to SEM stubs and secured on three perpendicular strips of conductive tape; fibers for cross-sectional imaging were secured to paper frames with a ~1 mm gap, submersed in liquid nitrogen for at least 1 min, and then folded to achieve a clean fracture of the fiber. Fractured fibers were then fixed on the SEM stub using a thick layer of conductive tape to allow vertical affixing of the fiber with the cross-section facing upward. SEM samples were sputter coated (EM ACE200; Leica Microsystems Inc.; Richmond Hill, ON) with Au/Pd particles (5 nm thickness). All images were collected using a LEO1455VP SEM (Carl Zeiss Canada) at 5000× magnification for surface imaging and 10 000× magnification for cross-sectional imaging.

**Raman Spectromicroscopy.** Raman spectromicroscopic measurements were collected similarly as done previously[22] with the use of a diffraction-limited Raman scattering design (modified from Gullekson et al.[35]) comprising an inverted Olympus IX71 optical microscope (Center Valley, PA) coupled to an iHR550 Raman spectrometer (Horiba Jobin Yvon; Edison, NJ). Spectra were recorded at ambient temperature and humidity for fibers produced under the AS and 2× EtOH stretched conditions. For each condition, Raman spectra were acquired using a 60× objective lens for three fibers at three disparate locations (10 scans, 20 s per scan) with the fiber both oriented at 0° and 90° relative to the polarization of the incident light using a confocal pinhole diameter of 400 $\mu$m and scanning from 900 to 1900 $cm^{-1}$. After data collection, spectra were analyzed using GRAMS/AI 9.0 (Thermo Scientific, Markham, ON). Each spectrum was baseline corrected, normalized, and $x$-axis corrected with respect to the phenylalanine band[16] at 1003 $cm^{-1}$, followed by averaging for a given condition and orientation relative to the incident polarization, with a final baseline correction of the averaged spectrum. During each day that measurements were carried out, a blank was recorded with the fiber far out of the observation area and, if needed, baseline subtraction was performed.

**Mechanical Testing.** Engineering stress−strain curves (i.e., determined taking into account fiber diameters prior to mechanical testing rather than "true" stress−strain curves that take into account changes in diameter during the testing process) were measured at room temperature and 50 ± 5% humidity using a home-built apparatus, as previously described.[23] Fibers were excluded based upon optical microscopy demonstrating abnormal surface morphology or outlying diameters that, correspondingly, exhibited mechanical properties that were exceedingly high (for diameters below ~27 $\mu$m for AS or below ~15 $\mu$m for 2× postspin stretching conditions) or exceedingly low (for diameters above ~40 $\mu$m for AS and ~20−21 $\mu$m for 2× postspin stretching conditions). The remaining stress−strain curves were analyzed to determine representative mechanical properties for a given condition. Data were processed as previously outlined,[23] with engineering stress and strain, toughness, and Young's modulus determined. Any fiber containing a property more than 2.5 standard deviations away from the average, without repetitive observation of this elevated or decreased behavior, was excluded from the final condition averages. Significance of differences between mechanical properties for disparate spinning conditions was evaluated using a two-tailed $t$-test with unequal variance.

## RESULTS AND DISCUSSION

**Recombinant Pyriform Silk Production and Purification.** The $HPy_2$ protein was readily expressed in *E. coli*, typically being enriched in the pellet versus the soluble fraction upon cell lysis and in subsequent workup (Figure 3). After trying a number of purification strategies, including use of immobilized-metal affinity chromatography (IMAC), a simple series of inclusion body washes was determined to be very effective. This provided a greater protein yield than IMAC with similar or better purity (Figure 3) through a relatively hands-off approach, very amenable to future scale-up of expression. The final protein yield ranged from ~24 mg per L of *E. coli* culture (following IMAC purification) to ~30−60 mg per L of *E. coli* culture (following the inclusion body wash method).

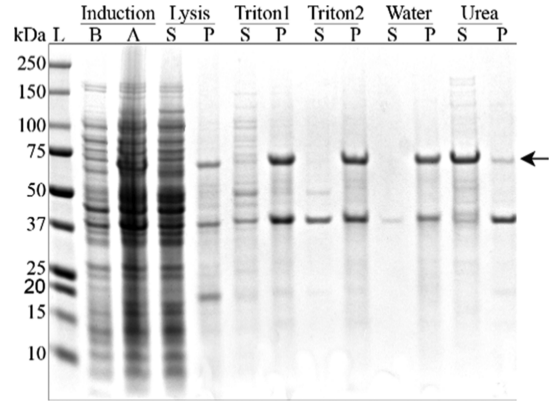


**Figure 3.** SDS-PAGE visualization of $HPy_2$ protein expression and purification. $HPy_2$ band migration is indicated by the black arrow; B and A are total cell before and after IPTG induction; S and P are soluble and pellet fractions at a given step: two Triton washes (Triton1, Triton2), a water wash to remove the Triton (water), and $HPy_2$ resuspension in 8 M urea (urea).

Based upon densitometry, $HPy_2$ purity is >70%; however, the caveat should be made that the $HPy_2$ sequence is well below average in its representation of any of the residues associated with Coomassie blue dye binding (namely, basic residues and aromatics;[36] comparative amino acid composition detailed in Table S1). Band intensity for $HPy_2$, on a molar basis, is therefore likely lower than for typical proteins. Hence, the densitometry-based estimate of purity should be regarded as a lower-bound, with actual purity likely higher.

Although the major protein overexpressed upon IPTG induction runs as a 65−70 kDa species based on SDS-PAGE (Figure 3), the primary protein solubilized in urea following Triton washes exhibits approximately the expected $HPy_2$ mass of 47.9 kDa (intact protein ESI+ MS; Figure S1). The identity of this protein was further confirmed through excision of the 65−70 kDa band and in-gel chymotryptic digestion, followed by ESI+ MS/MS with peptide fragments covering a wide range of the Gln-rich and the Pro-rich regions (Figure S2). The anomalous SDS-PAGE migration is, thus, likely due to high Pro content.[37] Namely, 38 of 477 residues are Pro, predominantly in the Pro-rich XP motif-containing segments (Figure 1). The major contaminating band was inferred to be a bacterial protein rather than a truncation product based on differing solution stability between $HPy_2$ and the 37 kDa band and the presence of this band in expression of other pyriform protein variants (data not shown).


DOI: 10.1021/acsbiomaterials.9b00504
ACS Biomater. Sci. Eng. 2019, 5, 4985−4993

**Spinning Dope Preparation and Characterization.** Based on precedents with single pyriform repeats[17] and widespread usage for silk spinning,[38] wet-spinning was targeted for formation of $HPy_2$ fibers. In wet-spinning, the protein in question must be solubilized at high concentration in a dope prior to extrusion through a spinneret into a coagulation bath. $HPy_2$ dissolved readily at ~10% (w/v) in a TFA/TFE/$H_2O$ (3:1:1 v/v/v) spinning dope that we recently developed for wet-spinning of recombinant aciniform silk fibers with a promising combination of strength and extensibility.[23] Interestingly, the 10% w/v $HPy_2$ TFA-based dope was more viscous (61.5 ± 6.2 mPa·s at 22.0 ± 0.1 °C) by ~2× relative to the corresponding TFA-based recombinant aciniform spidroin dope (31.3 ± 0.9 mPa·s for a 10% dope of the ~60 kDa molecular weight "$W_3$" protein[23]). This increased viscosity would be consistent with a lower degree of protein self-assembly relative to $W_3$, a greater degree of molecular entanglement and/or of formation of smaller self-assembled species in the $HPy_2$ versus $W_3$ dope.

As with the analysis using EMBOSS/GOR-based[39,40] secondary structure prediction reported by Chaw et al. for the PySp1 repetitive domain,[10] $HPy_2$ is predicted by EMBOSS/GOR to have a predominantly random coil (~53%) and β-sheet (~33%) content, with the remainder predicted to be β-turn (~5%) and α-helix (~9%). In contrast to this, the PSIPRED algorithm[24,25] predicts $HPy_2$ to be a mixed α-helical (~53%) and disordered (~47%) protein, with no β-sheet content. Consistent with the PSIPRED-predicted lack of β-sheet structuring, Raman spectromicroscopy of the dope in the *N. clavipes* pyriform gland setting estimated a helical content of 45 ± 3% and no β-strand content.[16]

Based on this dramatic variability in structural prediction as a function of algorithm, we examined the secondary structuring of $HPy_2$ in both phosphate buffer and in the TFA-based spinning dope using far-UV CD spectroscopy (Figure 4).

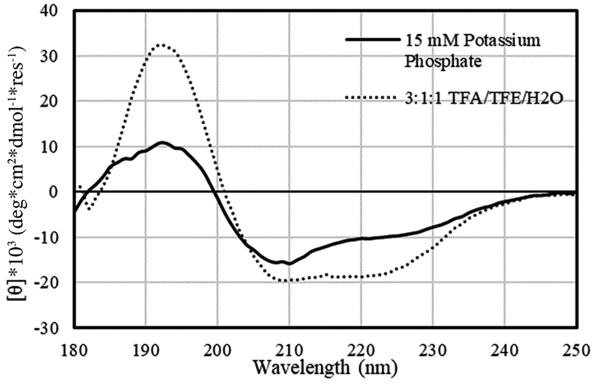


**Figure 4.** Far-UV CD spectra for $HPy_2$ in indicated conditions at 22.50 ± 0.05 °C.

Negative bands at 222 and 208 nm are consistent with $HPy_2$ having significant α-helical content in the spinning dope, with relatively minimal β-strand composition.[41] The protein exhibits a greater degree of helicity in the spinning dope relative to the potassium phosphate buffer, where the decreased magnitude of ellipticity observed at 190 and 220 nm in buffer may be explained by convolution with characteristic bands[41] arising from polyproline-II helices formed in Pro-rich motifs in phosphate buffer.

Using the BeStSel CD spectral deconvolution algorithm,[32,33] the higher α-helical character in the spinning dope versus buffer is supported (~41% in dope vs ~24% in buffer), with the presence of some (~13−14%) β-sheet content inferred in both conditions and the remainder being turn (9−12%) and disordered ("other") structures (Table S2). It should be noted that BeStSel deconvolution provides a more robust fit for the experimental data for $HPy_2$ in the dope solvent than in potassium phosphate buffer (Figure S3). As the polyproline-II band structure is not factored into the BeStSel algorithm,[32,33] the poorer deconvolution fit (e.g., the deviations in experimentally observed ellipticity at 208 and 220 nm versus those predicted by deconvolution) observed in buffer may be due at least in part to the presence of polyproline-II. Further experimental characterization would be needed to unequivocally test for the presence of polyproline-II in this protein. In short, CD spectroscopy is consistent with a mixed helical-random coil dope solution, with only modest β-sheet composition, following PSIPRED predictions and echoing Raman spectroscopy estimates in the native spinning dope.

**Silk Fiber Morphology, Structure, and Mechanics.** Wet-spinning was readily achieved using the above-noted dope of 10% $HPy_2$ in TFA/TFE/$H_2O$ (3:1:1 v/v/v), with an EtOH/$H_2O$ (9:1 v/v) coagulation bath. Silk-like fibers were collected in the AS state through spooling immediately following the coagulation bath (Figure 2a) or were subjected to an automated postspin stretching process, with a postspin draw ratio of 2× in three conditions: (1) in air (Figure 2b); (2) in air following immersion in EtOH/$H_2O$ (2:3 v/v; Figure 2c); or, (3) in EtOH/$H_2O$ (2:3 v/v; Figure 2d). Optical microscopy clearly demonstrates the expected significant diameter decrease (~31 to ~17−18 μm) on postspin stretching (Figure 5, light microscopy; Table 1; statistical comparison in Table S3), with relatively consistent diameters observed for fibers within a set. A qualitative increase in anisotropy was apparent between the AS state and any of the postspun stretching conditions (Figure 5, polarized light microscopy). Anisotropy further increases as a function of postspin stretching conditions, with the degree of anisotropy induced by stretching in air being the least, induced anisotropy upon EtOH immersion immediately prior to stretching being intermediate, and stretching in EtOH inducing the greatest degree of anisotropy.

Further insight into fiber structure and changes in structuring occurring between spinning conditions was provided by Raman spectromicroscopy [Figure 6 (averaged) and Figure S4 (overlaid)]. Examination of amide I band features for fibers produced at the extreme spinning conditions with regard to anisotropy—namely, the AS and 2× stretching in EtOH/$H_2O$ conditions—qualitatively implies that fibers were predominantly β-sheet, with depletion of α-helical content upon postspin stretching in EtOH/$H_2O$ relative to the AS state. Raman spectra were practically indistinguishable regardless of whether a given fiber was oriented parallel versus perpendicular to the polarization of the incident light. Given that some other Raman bands exhibit orientational anisotropy (Figure 6), the lack of orientation sensitivity of the amide I band may be due to a lesser degree of structural anisotropy than in, for example, wet-spun recombinant aciniform silk.[21−23] This requires further investigation through, for example, fully orientation-sensitive Raman spectromicroscopy[21] or fiber X-ray diffraction.[19] At present, it is apparent that each spinning condition leads to a distinct secondary structuring in the fiber


DOI: 10.1021/acsbiomaterials.9b00504
ACS Biomater. Sci. Eng. 2019, 5, 4985−4993

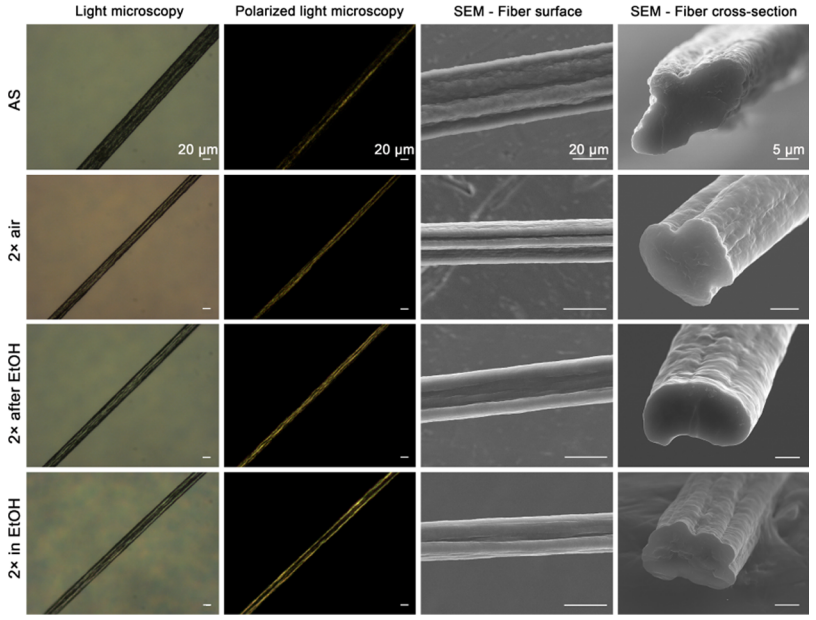


**Figure 5.** Representative optical microscopy, polarized light microscopy, and SEM micrographs for wet-spun recombinant pyriform silk either AS or with a 2× postspin stretch under the indicated stretching condition. Scale bars remain consistent for each column of images.

**Table 1. Mechanical Properties for Wet-Spun $HPy_2$ Fibers either in the AS State or with a 2× Postspin Stretch under the Indicated Stretching Condition (Mean ± Standard Deviation for *n* Fibers of a Given Type)**

| fiber type | strength (MPa) | extensibility (%) | toughness ($MJ \cdot m^{-3}$) | Young's modulus (GPa) | diameter ($\mu m$) | *n* |
|---|---|---|---|---|---|---|
| AS | 32.2 ± 7.4 | 3.3 ± 0.5 | 0.57 ± 0.19 | 1.30 ± 0.24 | 32.9 ± 4.5 | 15[a] |
| 2× air | 53.9 ± 9.7 | 4.6 ± 1.2 | 1.7 ± 0.70 | 1.96 ± 0.32 | 18.5 ± 1.6 | 17[b] |
| 2× after EtOH | 71.6 ± 5.6 | 15.6 ± 5.5 | 10.0 ± 3.7 | 2.92 ± 0.33 | 17.6 ± 1.0 | 12[c] |
| 2× in EtOH | 65.9 ± 8.6 | 27.6 ± 6.1 | 16.7 ± 4.0 | 2.61 ± 0.34 | 18.0 ± 1.4 | 8[d] |

[a]No data sets with anomalous mechanical properties observed. [b]One mechanical data set excluded due to anomalously high extensibility (~11%; Figure S5b). [c]Two data sets excluded due to anomalously high extensibilities (~48−62%); one due to anomalously low strength (~42 MPa); one due to anomalously high toughness (~25 $MJ \cdot m^{-3}$); all anomalous data presented in Figure S5c. [d]One mechanical data set excluded due to anomalously low extensibility (~5%; Figure S5d).

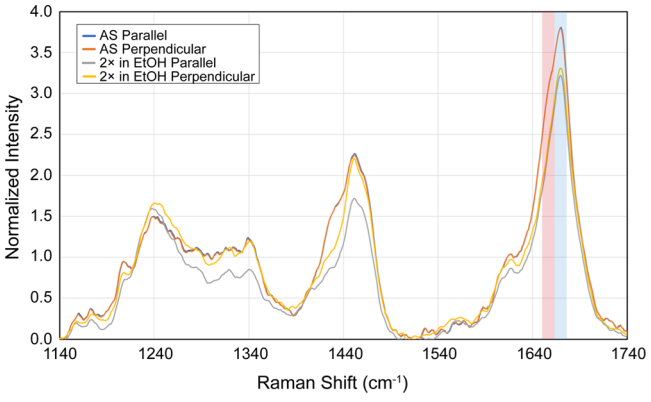


**Figure 6.** Raman spectroscopy results of AS fibers and fibers stretched 2× in EtOH acquired with the fiber long axis oriented as noted to the incident laser polarization. Typical Raman band regions[16] for $\alpha$-helix (red) and $\beta$-sheet (blue) shown as shaded bars.

state, with postspin stretching in $EtOH/H_2O$ leading to further enrichment of $\beta$-sheet relative to $\alpha$-helix with respect to the AS condition.

Providing greater context, the mechanical behavior of wet-spun $HPy_2$ fibers was also extremely condition-dependent (Table 1; Figure 7 (individual fibers); Figure S5 (individual fibers including those with anomalous mechanics); Figure 8 (representative data); statistical comparisons in Tables S3−S5). Namely, postspin stretching approximately doubled fiber strength, with extensibility significantly improved by all postspin stretching conditions (Table S4). Postspin stretching employing 2:3 $EtOH/H_2O$ further enhanced extensibility. Stretching in or following immersion in $EtOH/H_2O$ provided the greatest strength, whereas stretching in $EtOH/H_2O$ provided the greatest extensibility and, correspondingly, toughness (Table S5). Young's modulus also increased significantly upon postspin stretching (Table S4), with the greatest increase for 2× stretching after solvent exposure. No clear correlation was observed between mechanical properties and diameter variations within a given condition (Figure 7).

The observed mechanical data are consistent with a situation where prolonged and continuous exposure to a solvent during the stretching process is helping to promote additional structural rearrangements in the fibers. Specifically, the $\alpha$-helical structure is being depleted, as implied by Raman spectromicroscopy (Figure 6). Potentially, this arises because of specific conversion to $\beta$-sheet; whereas our Raman spectromicroscopy apparatus does not allow for full spectral decomposition and secondary structure analysis, this would help to explain the near doubling in strength observed with postspin stretching. A higher degree of structural rearrangement is also supported by polarized light microscopy, with


DOI: 10.1021/acsbiomaterials.9b00504
ACS Biomater. Sci. Eng. 2019, 5, 4985−4993

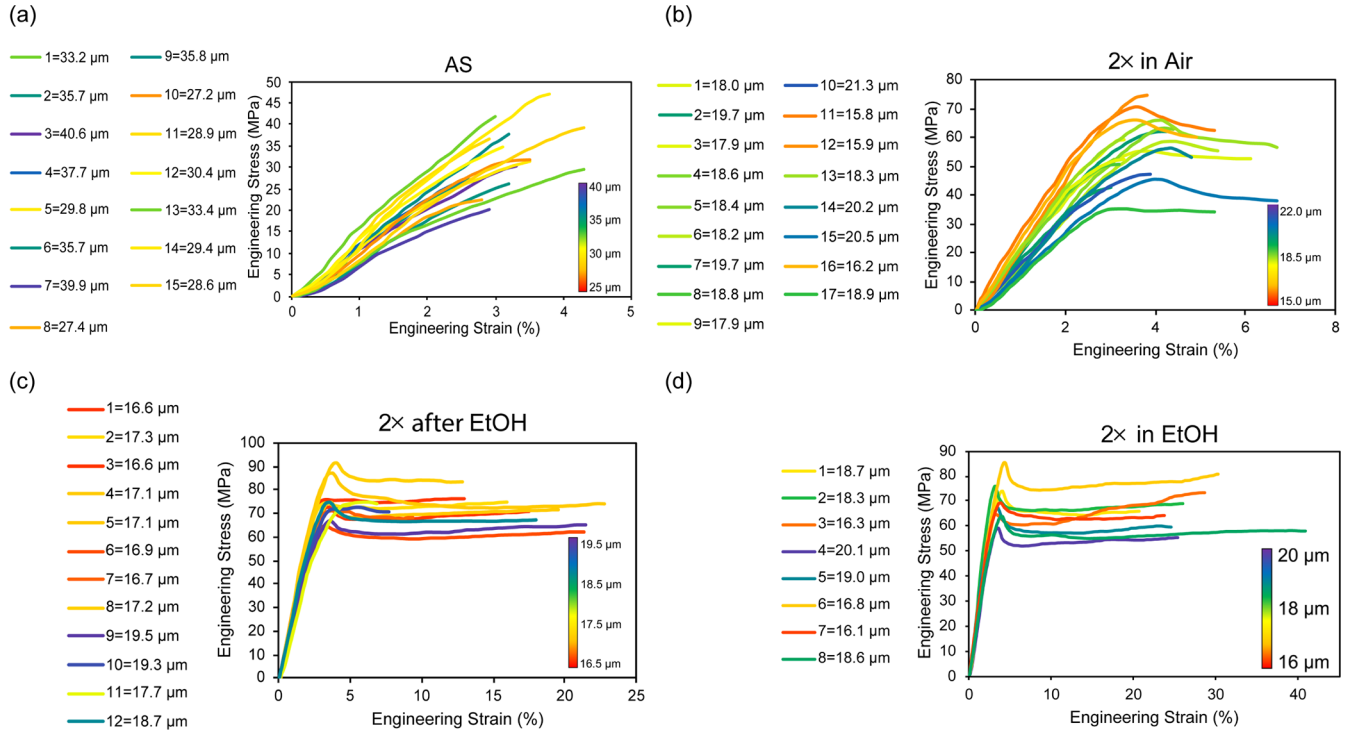


**Figure 7.** Stress–strain curves for each individual fiber included in mechanical data averages (Table 1) color-coded by fiber diameter (individual color scales shown in each panel with actual diameters for each fiber denoted in legend).

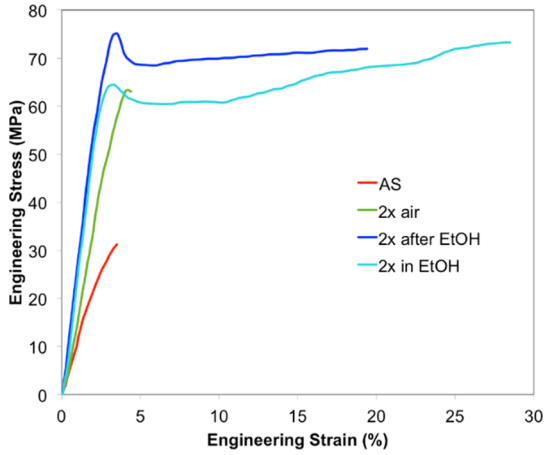


**Figure 8.** Representative stress–strain curves for $HPy_2$ fibers wet-spun under indicated condition.

greater anisotropy observed as a function of solvent exposure (Figure 5).

Given the noncylindrical appearance of $HPy_2$ fibers by SEM (Figure 5), it should be noted that SEM micrograph analysis indicated that the longer cross-sectional diameter for AS, 2× air stretched, and 2× stretched in EtOH/$H_2O$ conditions was closer to the average measured by optical microscopy (Table 1) than the shorter diameter. The opposite held true for fibers stretched 2× following EtOH/$H_2O$ immersion. As diameter is integral to calculation of stress, this implies that the reported values for engineering stress are likely to be systematically lower than the true value for the former conditions, whereas fibers stretched 2× after EtOH/$H_2O$ immersion may not be as strong as indicated, leading to some ambiguity on the level of impact stretching in or after the EtOH/$H_2O$ bath had with regard to strength. Although ideally the irregular noncylindrical cross-sections observed could be accounted for, it is not possible to use the same sample for both mechanical testing and the SEM cross-sectional analysis required to accurately measure noncylindrical geometry; hence, optical microscopy was employed to allow for direct diameter estimation of samples employed in mechanical testing despite the noted limitations in stress determination.

**Comparison to Other Silks.** Based on the stress–strain analysis, recombinant pyriform silk fibers exhibit a favorable combination of both strength and extensibility. Comparing $HPy_2$ fibers with regenerated *B. mori* silk processed likewise,[34] the regenerated silkworm silk is slightly stronger, while exhibiting an extensibility ∼one-third that of $HPy_2$. Moving to recombinant spider silks, the strength of recombinant silk fibers generally increases as a function of spidroin molecular weight, as shown, for example, with both aciniform[22] and dragline[42] silks. We thus compare the properties of the ∼47.9 kDa $HPy_2$ silk to previously reported wet-spun silk fibers produced from recombinant spidroins of similar molecular weight. In comparison to ∼60 kDa recombinant aciniform spidroin spun from the same dope,[23] lower strength and extensibility are observed for $HPy_2$. Conversely, $HPy_2$ silk fibers exhibit comparable strength to and greater extensibility than an ∼54.6 kDa recombinant dragline silk.[42] Similarly, wet-spun fibers from the repetitive domain of recombinant tubuliform silk (fused to N-terminal thioredoxin- and C-terminal $His_6$-tags, total molecular weight ≈ 33 kDa) exhibit slightly higher strength but lower extensibility[19] than $HPy_2$ fibers. Finally, $HPy_2$ fibers show similar strength and much greater extensibility than most of a series of wet-spun recombinant flagelliform silks ranging from 47 to 99 kDa.[43]

Following from the hypothesis of Lefèvre et al.[16] (vide supra) that pyriform and aciniform silk would have comparable behavior based on structural inferences from Raman



DOI: 10.1021/acsbiomaterials.9b00504
ACS Biomater. Sci. Eng. 2019, 5, 4985–4993

spectromicroscopy, recombinant pyriform silk does indeed exhibit a similar combination of strength and extensibility to aciniform silk. It also exhibits greater extensibility than dragline silk, as would be anticipated if the behavior of pyriform silk is akin to the very tough aciniform silk.[11] The combination of strength and extensibility observed in wet-spun pyriform silk, thus, imply a naturally-tough silk. The dramatic variation in mechanical behavior observed as a function of postspin stretching conditions is also notable, implying that design of further protein constructs and modulation of spinning conditions are both likely routes to enhance recombinant pyriform silk mechanical properties.

With further investigation into pyriform glue, recombinant pyriform silk mechanical properties could be enhanced even further. Wolff et al.[7] hypothesized that strong cohesion occurs between the glue and silk proteins through ionic and dipole−dipole interactions. Although we have shown that recombinant pyriform silk alone can be strong and extensible, its natural functioning as part of a hierarchically structured attachment disc indicates that its properties could be modulated even further through exposure to glue protein or an environment mimicking that provided by the glue protein environment during the spinning process.

## CONCLUSIONS

Although not yet probing a naturally produced pyriform silk, this work provides the first insight into the mechanical properties of this class of silk. We have shown that recombinant proteins based on the pyriform silk repetitive domain can be produced with both good purity and yield while appearing to have significant $\alpha$-helical content in the solution-state, consistent with Raman spectromicroscopy in the native gland.[16] This recombinant silk protein was capable of forming strong fibers, with tunable extensibility based upon solvent exposure during postspin stretching. In turn, this may correspond to the variation of pyriform silk function required for application in different attachment disc architectures.[8,9] Changes in properties as a function of postspin stretching and solvent exposure were reflected in mechanical behavior, through optical microscopy, with greater molecular anisotropy on solvent exposure and through loss in $\alpha$-helical content on postspin stretching. Each piece of evidence indicated that clear, mechanically advantageous structural changes were occurring. The observed tunability of mechanical behavior also implies other approaches (e.g., change in solvent employed during post-spin stretching), which could further improve the properties of this strong and extensible recombinant silk.

## ASSOCIATED CONTENT

### Supporting Information

The Supporting Information is available free of charge on the ACS Publications website at DOI: 10.1021/acsbiomaterials.9b00504.

MS deconvolution and MS/MS peptide fragment mapping; CD deconvolution results; overlaid Raman spectral data; amino acid composition comparison; and statistical comparison of fiber diameters and mechanical properties (PDF)

## AUTHOR INFORMATION

### Corresponding Author

*E-mail: jan.rainey@dal.ca.

### ORCID

Jan K. Rainey: 0000-0003-0793-5573

### Funding

This work was supported by a Natural Sciences and Engineering Research Council of Canada (NSERC) Discovery Grant (RGPIN/05907-2017), an NSERC Discovery Accelerator Supplement (RGPAS/507805-2017), the NSERC CREATE Training Program in BioActives (510963), and by equipment and infrastructure grants from NSERC, the Canadian Foundation for Innovation, and the Dalhousie Medical Research Foundation.

### Notes

The authors declare no competing financial interest.

## ACKNOWLEDGMENTS

We would like to thank Nathan Weatherbee-Martin and Denis Baev for engineering and set up of the spinning apparatus; Bruce Stewart for expert assistance; John Noddin and Kevin Borgel (Department of Physics & Atmospheric Science Machine Shop, Dalhousie University) for apparatus design and fabrication; Dr. Laurent Kreplak for Raman spectromicroscope access and assistance (Department of Physics & Atmospheric Science, Dalhousie University); Dr. Ping Li (Scientific Imaging Suite, Dalhousie University) for SEM support and access; and, Dr. Alejandro Cohen (Proteomics and MS Core Facility, Dalhousie University) for performing MS and analysis.

## REFERENCES

(1) Andersen, S. O. Amino acid composition of spider silks. *Comp. Biochem. Physiol.* **1970**, *35*, 705−711.

(2) Hayashi, C. Y.; Lewis, R. V. Evidence from flagelliform silk cDNA for the structural basis of elasticity and modular nature of spider silks. *J. Mol. Biol.* **1998**, *275*, 773−784.

(3) Vollrath, F.; Edmonds, D. T. Modulation of the mechanical properties of spider silk by coating with water. *Nature* **1989**, *340*, 305.

(4) Zhao, J.; Lv, B.; Zhang, F.; Yang, Z.; Qian, L.; Chen, C.; Long, X. Effects of austempering temperature on bainitic microstructure and mechanical properties of a high-C high-Si steel. *Mater. Sci. Eng., A* **2019**, *742*, 179−189.

(5) Gosline, J. M.; Guerette, P. A.; Ortlepp, C. S.; Savage, K. N. The mechanical design of spider silks: from fibroin sequence to mechanical function. *J. Exp. Biol.* **1999**, *202*, 3295−3303.

(6) Kovoor, J.; Zylberberg, L. Fine structural aspects of silk secretion in a spider (*Araneus diadematus*). I. Elaboration in the pyriform glands. *Tissue Cell* **1980**, *12*, 547−556.

(7) Wolff, J. O.; Grawe, I.; Wirth, M.; Karstedt, A.; Gorb, S. N. Spider's super-glue: thread anchors are composite adhesives with synergistic hierarchical organization. *Soft Matter* **2015**, *11*, 2394−2403.

(8) Sahni, V.; Harris, J.; Blackledge, T. A.; Dhinojwala, A. Cobweb-weaving spiders produce different attachment discs for locomotion and prey capture. *Nat. Commun.* **2012**, *3*, 1106.

(9) Wirth, M.; Wolff, J. O.; Appel, E.; Gorb, S. N. Ultrastructure of spider thread anchorages. *J. Morphol.* **2019**, *280*, 534−543.

(10) Chaw, R. C.; Saski, C. A.; Hayashi, C. Y. Complete gene sequence of spider attachment silk protein (PySp1) reveals novel linker regions and extreme repeat homogenization. *Insect Biochem. Mol. Biol.* **2017**, *81*, 80−90.

(11) Hayashi, C. Y.; Blackledge, T. A.; Lewis, R. V. Molecular and mechanical characterization of aciniform silk: uniformity of iterated sequence modules in a novel member of the spider silk fibroin gene family. *Mol. Biol. Evol.* **2004**, *21*, 1950−1959.



DOI: 10.1021/acsbiomaterials.9b00504
*ACS Biomater. Sci. Eng.* 2019, 5, 4985−4993

(12) Ayoub, N. A.; Garb, J. E.; Tinghitella, R. M.; Collin, M. A.; Hayashi, C. Y. Blueprint for a high-performance biomaterial: full-length spider dragline silk genes. *PLoS One* **2007**, *2*, No. e514.
(13) Hayashi, C. Y.; Shipley, N. H.; Lewis, R. V.; Lewis, R. V. Hypotheses that correlate the sequence, structure, and mechanical properties of spider silk proteins. *Int. J. Biol. Macromol.* **1999**, *24*, 271−275.
(14) Colgin, M. A.; Lewis, R. V. Spider minor ampullate silk proteins contain new repetitive sequences and highly conserved non-silk-like "spacer regions". *Protein Sci.* **1998**, *7*, 667−672.
(15) Chaw, R. C.; Collin, M.; Wimmer, M.; Helmrick, K.-L.; Hayashi, C. Y. Egg case silk gene sequences from *Argiope* spiders: evidence for multiple loci and a loss of function between paralogs. *G3: Genes, Genomes, Genet.* **2018**, *8*, 231−238.
(16) Lefèvre, T.; Boudreault, S.; Cloutier, C.; Pézolet, M. Diversity of molecular transformations involved in the formation of spider silks. *J. Mol. Biol.* **2011**, *405*, 238−253.
(17) Geurts, P.; Zhao, L.; Hsia, Y.; Gnesa, E.; Tang, S.; Jeffery, F.; Mattina, C. L.; Franz, A.; Larkin, L.; Vierra, C. Synthetic Spider Silk Fibers Spun from Pyriform Spidroin 2, A Glue Silk Protein Discovered in Orb-Weaving Spider Attachment Discs. *Biomacromolecules* **2010**, *11*, 3495−3503.
(18) Andersson, M.; Chen, G.; Otikovs, M.; Landreh, M.; Nordling, K.; Kronqvist, N.; Westermark, P.; Jörnvall, H.; Knight, S.; Ridderstråle, Y.; Holm, L.; Meng, Q.; Jaudzems, K.; Chesler, M.; Johansson, J.; Rising, A. Carbonic anhydrase generates $CO_2$ and $H^+$ that drive spider silk formation via opposite effects on the terminal domains. *PLoS Biol.* **2014**, *12*, No. e1001921.
(19) Gnesa, E.; Hsia, Y.; Yarger, J. L.; Weber, W.; Lin-Cereghino, J.; Lin-Cereghino, G.; Tang, S.; Agari, K.; Vierra, C. Conserved C-terminal domain of spider tubuliform spidroin 1 contributes to extensibility in synthetic fibers. *Biomacromolecules* **2012**, *13*, 304−312.
(20) Ittah, S.; Michaeli, A.; Goldblum, A.; Gat, U. A model for the structure of the C-terminal domain of dragline spider silk and the role of its conserved cysteine. *Biomacromolecules* **2007**, *8*, 2768−2773.
(21) Xu, L.; Lefèvre, T.; Orrell, K. E.; Meng, Q.; Auger, M.; Liu, X.-Q.; Rainey, J. K. Structural and mechanical roles for the C-terminal nonrepetitive domain become apparent in recombinant spider aciniform silk. *Biomacromolecules* **2017**, *18*, 3678−3686.
(22) Weatherbee-Martin, N.; Xu, L.; Hupe, A.; Kreplak, L.; Fudge, D. S.; Liu, X.-Q.; Rainey, J. K. Identification of wet-spinning and post-spin stretching methods amenable to recombinant spider aciniform silk. *Biomacromolecules* **2016**, *17*, 2737−2746.
(23) Xu, L.; Weatherbee-Martin, N.; Liu, X. Q.; Rainey, J. K. Recombinant Silk Fiber Properties Correlate to Prefibrillar Self-Assembly. *Small* **2019**, *15*, 1805294.
(24) Buchan, D. W. A.; Minneci, F.; Nugent, T. C. O.; Bryson, K.; Jones, D. T. Scalable web services for the PSIPRED Protein Analysis Workbench. *Nucleic Acids Res.* **2013**, *41*, W349−W357.
(25) Jones, D. T. Protein secondary structure prediction based on position-specific scoring matrices. *J. Mol. Biol.* **1999**, *292*, 195−202.
(26) Xu, L.; Rainey, J. K.; Meng, Q.; Liu, X.-Q. Recombinant minimalist spider wrapping silk proteins capable of native-like fiber formation. *PLoS One* **2012**, *7*, No. e50227.
(27) Tremblay, M.-L.; Xu, L.; Lefèvre, T.; Sarker, M.; Orrell, K. E.; Leclerc, J.; Meng, Q.; Pézolet, M.; Auger, M.; Liu, X.-Q.; Rainey, J. K. Spider wrapping silk fibre architecture arising from its modular soluble protein precursor. *Sci. Rep.* **2015**, *5*, 11502.
(28) Schnaitman, C. A. Solubilization of the cytoplasmic membrane of *Escherichia coli* by Triton X-100. *J. Bacteriol.* **1971**, *108*, 545−552.
(29) Bordier, C. Phase separation of integral membrane proteins in Triton X-114 solution. *J. Biol. Chem.* **1981**, *256*, 1604−1607.
(30) Shevchenko, A.; Tomas, H.; Havli, J.; Olsen, J. V.; Mann, M. In-gel digestion for mass spectrometric characterization of proteins and proteomes. *Nat. Protoc.* **2006**, *1*, 2856−2860.
(31) Kuipers, B. J. H.; Gruppen, H. Prediction of Molar Extinction Coefficients of Proteins and Peptides Using UV Absorption of the Constituent Amino Acids at 214 nm To Enable Quantitative Reverse Phase High-Performance Liquid Chromatography−Mass Spectrometry Analysis. *J. Agric. Food Chem.* **2007**, *55*, 5445−5451.
(32) Micsonai, A.; Wien, F.; Bulyáki, É.; Kun, J.; Moussong, É.; Lee, Y.-H.; Goto, Y.; Réfrégiers, M.; Kardos, J. BeStSel: a web server for accurate protein secondary structure prediction and fold recognition from the circular dichroism spectra. *Nucleic Acids Res.* **2018**, *46*, W315−W322.
(33) Micsonai, A.; Wien, F.; Kernya, L.; Lee, Y.-H.; Goto, Y.; Réfrégiers, M.; Kardos, J. Accurate secondary structure prediction and fold recognition for circular dichroism spectroscopy. *Proc. Natl. Acad. Sci. U.S.A.* **2015**, *112*, E3095−E3103.
(34) Zhou, G.; Shao, Z.; Knight, D. P.; Yan, J.; Chen, X. Silk Fibers Extruded Artificially from Aqueous Solutions of Regenerated *Bombyx mori* Silk Fibroin are Tougher than their Natural Counterparts. *Adv. Mater.* **2009**, *21*, 366−370.
(35) Gullekson, C.; Lucas, L.; Hewitt, K.; Kreplak, L. Surface-sensitive Raman spectroscopy of collagen I fibrils. *Biophys. J.* **2011**, *100*, 1837−1845.
(36) Brady, P. N.; Macnaughtan, M. A. Evaluation of colorimetric assays for analyzing reductively methylated proteins: Biases and mechanistic insights. *Anal. Biochem.* **2015**, *491*, 43−51.
(37) Hames, B. D. *Gel Electrophoresis of Proteins: A Practical Approach*, 3rd ed.; Oxford University Press Inc.: New York 1998.
(38) Koeppel, A.; Holland, C. Progress and trends in artificial silk spinning: a systematic review. *ACS Biomater. Sci. Eng.* **2017**, *3*, 226−237.
(39) Garnier, J.; Osguthorpe, D. J.; Robson, B. Analysis of the accuracy and implications of simple methods for predicting the secondary structure of globular proteins. *J. Mol. Biol.* **1978**, *120*, 97−120.
(40) Rice, P.; Longden, I.; Bleasby, A. EMBOSS: the European molecular biology open software suite. *Trends Genet.* **2000**, *16*, 276−277.
(41) Greenfield, N. J. Methods to estimate the conformation of proteins and polypeptides from circular dichroism data. *Anal. Biochem.* **1996**, *235*, 1−10.
(42) Xia, X.-X.; Qian, Z.-G.; Ki, C. S.; Park, Y. H.; Kaplan, D. L.; Lee, S. Y. Native-sized recombinant spider silk protein produced in metabolically engineered *Escherichia coli* results in a strong fiber. *Proc. Natl. Acad. Sci. U.S.A.* **2010**, *107*, 14059−14063.
(43) Li, X.; Shi, C.-H.; Tang, C.-L.; Cai, Y.-M.; Meng, Q. The correlation between the length of repetitive domain and mechanical properties of the recombinant flagelliform spidroin. *Biol. Open* **2017**, *6*, 333−339.


DOI: 10.1021/acsbiomaterials.9b00504
*ACS Biomater. Sci. Eng.* 2019, 5, 4985−4993